

See discussions, stats, and author profiles for this publication at: <https://www.researchgate.net/publication/26809123>

Toward Understanding Metal-Binding Specificity of Porphyrin: A Conceptual Density Functional Theory Study

ARTICLE *in* THE JOURNAL OF PHYSICAL CHEMISTRY B · SEPTEMBER 2009

Impact Factor: 3.3 · DOI: 10.1021/jp905885y · Source: PubMed

CITATIONS

20

READS

65

5 AUTHORS, INCLUDING:



Ming Lei

Beijing University of Chemical Technology

57 PUBLICATIONS 434 CITATIONS

[SEE PROFILE](#)



Wei-Hai Fang

Beijing Normal University

233 PUBLICATIONS 4,415 CITATIONS

[SEE PROFILE](#)



Shubin Liu

University of North Carolina at Chapel Hill

154 PUBLICATIONS 5,306 CITATIONS

[SEE PROFILE](#)

Toward Understanding Metal-Binding Specificity of Porphyrin: A Conceptual Density Functional Theory Study

Xin-Tian Feng,[†] Jian-Guo Yu,^{*,†} Ming Lei,[‡] Wei-Hai Fang,[†] and Shubin Liu^{*,§}

Department of Chemistry, Beijing Normal University, Beijing 100875, PR China, Institute of Materia Medica and Department of Chemistry, School of Science, Beijing University of Chemical Technology, Beijing 100029 PR China, and Research Computing Center, University of North Carolina, Chapel Hill, North Carolina 27599-3420

Received: June 23, 2009; Revised Manuscript Received: August 13, 2009

Porphyrin is a key cofactor of hemoproteins. The complexes it forms with divalent metal cations such as Fe, Mg, and Mn compose an important category of compounds in biological systems, serving as a reaction center for a number of essential life processes. Employing density functional theory (DFT) and conceptual DFT approaches, the structural properties and reactivity of (*pyridine*)_{*n*}—M—porphyrin complexes were systematically studied for the following selection of divalent metal cations: Mg, Ca, Cr, Mn, Co, Ni, Cu, Zn, Ru, and Cd with *n* varying from 0, 1, to 2. Metal selectivity and porphyrin specificity were investigated from the perspective of both structural and reactivity properties. Quantitative structural and reactivity relationships have been discovered between bonding interactions, charge distributions, and DFT chemical reactivity descriptors. These results are beneficial to our understanding of the chemical reactivity and metal cation specificity for heme-containing enzymes and other metalloproteins alike.

1. Introduction

Due to their abundance in nature and the essential roles they play in physiological processes as sensors, activators, and carriers of gaseous molecules, hemoproteins such as hemoglobin,^{1,2} myoglobin,^{3,4} hemocyanin,^{5–7} and neuroglobin⁸ comprise some of the most well understood proteins in terms of structure, function, and evolution in protein families.^{9,10} As the core cofactor of hemoproteins, heme is a metal-binding porphyrin consisting of a heterocyclic organic ring made from four pyrrole subunits linked via methine bridges. It serves as a prosthetic group for many biological processes including oxidative metabolism,^{11–13} xenobiotic detoxification, the synthesis and sensing of diatomic gases, cellular differentiation, gene regulation at the level of transcription, protein translation and targeting, and protein stability. Hemoglobin is most commonly found in its oxygen-binding state where the bonded metal cation is a divalent iron. Other porphyrin-binding divalent metal ions have also been found such as Mn (chloroperoxidase),¹⁴ Mg (chlorophyll),¹⁵ Zn (Zn—protoporphyrin IX),¹⁶ Cr (chromium mesoporphyrin),¹⁷ Cu (hemocyanins),⁷ etc. When in its resting or functioning state, up to two axial ligands are required to bond with the metal cation in the metal—porphyrin complex to carry out the catalytic process. The most common axial residues in hemoproteins are histidine and cysteine.

For metalloproteins to properly function under physiological conditions, selective and specific binding of appropriate metal cations is necessary. For example, calcium ions bind to EF-hand proteins^{18–20} and zinc ions bind to zinc-finger motifs.^{21–25} Incorporation of inappropriate metal ions in these species can have detrimental consequences. Since the inner cavity of the porphyrin ring is relatively large, hemoproteins can form peripherally metalated complexes with many different metal

ions. This promiscuous metal-binding property of porphyrin does not mean, however, that it has no specificity or selectivity. To illustrate, no calcium-binding hemoproteins have ever been detected in nature. What is the cause of this absence? Also, why is the iron ion preferred over others in hemoproteins? It is commonly believed that the metal-binding specificity is dictated by the microscopic surrounding environment of the metal-binding site, where both thermodynamically and kinetically controlled mechanisms together with working principles, like the hard/soft acid base effect,^{11,12} govern metal specificity.

In our present work, we explored the metal-binding selectivity and specificity of porphyrin from the perspective of structure and reactivity properties. Toward that end, together with conventional DFT methods, we utilized the framework of conceptual DFT, which has recently been of considerable interest in the literature toward understanding chemical reactivity.^{26–28} The ultimate question we wanted to answer is the following: What are the structural, electronic, or stereoelectronic factors that govern porphyrin's specific metal ion binding capability and are involved in the performance of biological functions under physiological conditions? In this work, we address a less demanding inquiry: Based on conceptual DFT, in the gas phase under vacuum, can we observe any behavior differences in structure and reactivity descriptors for the porphyrin complexes in bonding with different metal cations and axial ligands?

2. Computational Details

The following 11 divalent metal cations will be employed in this study for the porphyrin—M(II) complex, with M = Fe, Mg, Ca, Cr, Mn, Co, Ni, Cu, Zn, Ru, and Cd. To study the impact of the axial ligands on structural and electronic properties of the complex, we used the six-membered pyridine ring (Py), with which we will consider cases with zero, one, and two pyridines axially bonded to the metal cation as the axial-binding models (Scheme 1). These binding models will be denoted p0, p1, and p2, respectively.

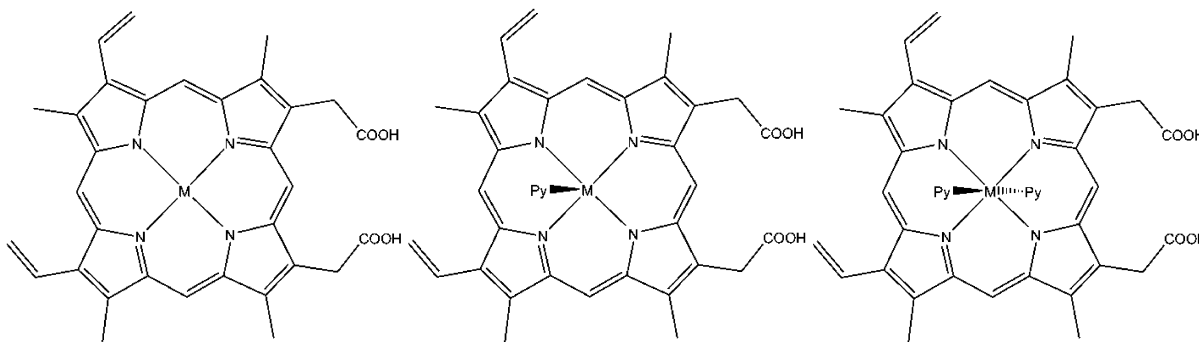
* To whom all correspondence should be addressed. E-mail addresses: jianguo_yu@bnu.edu.cn (JGY) and shubin@email.unc.edu (SBL).

[†] Beijing Normal University.

[‡] Beijing University of Chemical Technology.

[§] University of North Carolina.

SCHEME 1: (Pyridine)_n—Metal—Porphyrin Systems Investigated in This Work, with M = Mg, Ca, Cr, Mn, Co, Ni, Cu, Zn, Ru, and Cd and n = 0, 1, and 2



In conceptual DFT,²⁶ the chemical potential, μ , and global hardness, η , are defined as the following derivatives: $\mu = (\partial E / \partial N)_v = -\chi$ and $\eta = (\partial^2 E / \partial N^2)_v = (\partial \mu / \partial N)_v$, respectively, where E is the total energy of the system, N the number of electrons, v the external potential, and χ electronegativity. According to Mulliken,²⁹ $\mu = -\chi = -(1/2)(I + A)$ and $\eta = I - A$ with I and A as the first ionization energy and electron affinity, respectively, which can be approximated by the HOMO and LUMO energies via $I \approx -\epsilon_{\text{HOMO}}$ and $A \approx -\epsilon_{\text{LUMO}}$.³⁰ Softness, S , is defined as the inverse of the hardness, $S = (1/2)\eta$, and the electrophilicity index,³¹ a measure of the lowering of the total binding energy due to the maximal electron acceptance, can be expressed in terms of μ and η as $\omega = (\mu^2/2\eta)$. Other conceptual DFT quantities such as nucleofugality, ΔE_n , and electrofugality, ΔE_e ,³² are defined as follows: $\Delta E_n \equiv -A + \omega = [(\mu + \eta)^2]/(2\eta)$ and $\Delta E_e = I + \omega = [(\mu - \eta)^2]/(2\eta)$. These global reactivity descriptors from the conceptual DFT framework, μ , η , ω , ΔE_n , and ΔE_e , will be used to appraise the global chemical reactivity of our systems.

To describe regioselectivity tendencies of individual atoms in molecules, local descriptors were employed. The first well-known example of such a category is called the Fukui function,^{26,27,33} defined as $f(r) = (\partial \rho(r) / \partial N)_v = (\partial \mu / \partial v(r))_N$ where $\rho(r)$ is the electron density. Yang and Mortier³⁴ have proposed that for systems with a gain of electrons the condensed Fukui index, $f_k^+ = q_k(N + 1) - q_k(N)$, in the finite difference approximation is a measure of nucleophilic attack, where $q_k(N)$ is the gross atomic charge for atom k with N electrons, obtained from a population analysis (such as NBO analysis). For systems that can donate electrons, the condensed Fukui index is susceptible to electrophilic attack with $f_k^- = q_k(N) - q_k(N - 1)$. For radical attack reactions, $f_k^0 = (1/2)(f_k^+ + f_k^-)$, where $q_k(N + 1)$, $q_k(N)$, and $q_k(N - 1)$ are the gross NBO population on atom k in a molecule with $N + 1$ (anion state), N (neutral state), and $N - 1$ (cation state) electrons, respectively. The local component of the softness reactivity indicator, the local softness, introduced by Parr and Yang as,³⁵ $s(r) = (\partial \rho(r) / \partial \mu)_v = (\partial \rho(r) / \partial N)_v (\partial N / \partial \mu)_v = Sf(r)$, has been widely used.³⁶ Similar to the Fukui function, within the finite difference approximation, the condensed form of these three local softness indicators for any particular atom k can be written as $s_k^+ = Sf_k^+$ (for nucleophilic attack), $s_k^- = Sf_k^-$ (for electrophilic attack), and $s_k^0 = Sf_k^0$ (for radical attack). Another kind of reactivity index, called the dual descriptor, has been proposed,³⁷ which serves as “an indicator for both the nucleophilic and electrophilic regions of a molecule”. Morell, Grand, and Toro-Labbe proposed the first dual descriptor using the cross-term third-order derivative $f^{(2)}(r) = (\partial^2 / \partial^2 N (\partial E / \partial v(r)))_N = (\partial^2 E / \partial v(r) \partial^2 N)_N = (\partial f(r) / \partial N)_v = (\partial \eta / \partial v(r))_N$, and under the finite difference approximation, one

gets $f^{(2)}(r) = f^+(r) - f^-(r)$. The dual descriptor, $f^{(2)}(r)$, will be positive in electrophilic regions where $\rho_{\text{LUMO}}(r)$ is large and negative in nucleophilic regions where $\rho_{\text{HOMO}}(r)$ dominates.

In addition to the global and local descriptors from conceptual DFT, we will also employ NBO analyses³⁸ to perform second-order perturbation analyses to understand the bonding features between the metal cation and the porphyrin ring and between the metal cation and the axially bonded pyridine groups.

All calculations were performed using the B3LYP^{39,40} functional and a compound basis set, where the 6-31G basis sets were used for the elements C and H, and Pople's 6-311+G(d) basis sets were used for N, O, and M (where M = Mg, Ca, Cr, Mn, Co, Ni, Cu, Zn).^{41,42} These generic basis sets⁴³ have previously proven to be effective⁴⁴ by being both efficient and reliable in predicting structural and reactive properties for heme-like systems. For Ru and Cd for which no Pople basis set is available, we used the ECP Stuggart basis set instead. For each system, we first performed a tight structural optimization, followed by a frequency calculation to confirm that the optimized structure was indeed a minimum (with no imaginary frequencies). Single-point frequency calculations and NBO analyses were carried out with tight SCF convergence and ultrafine grids in the structural optimizations. For metal ions with different spin states, each multiplicity was examined, and the spin state with the lowest energy was then chosen for subsequent study. The effectiveness of the present approach in dealing with spin multiplicity under the framework of DFT has been addressed earlier.⁴⁵ All calculations were performed using the Gaussian 03 package version E01.⁴⁶

3. Results and Discussion

Table 1 shows a few key structural parameters of the three classes of (pyridine)_n—metal—porphyrin complexes (Scheme 1) with 11 different divalent metal ions and varying numbers of axial pyridine groups ($n = 0, 1, 2$). Also shown in the table is the multiplicity of the lowest-energy spin state⁴⁴ and the divalent ionic radius of the metal cation. One can see that for the majority of complexes the bond length between the metal cation and porphyrin nitrogen atom, M—N(Pph), the metal ion and pyridine nitrogen atom, M—N(Py), and the metal ion and porphyrin plane, M—Plane, for p0—p2 classes are very similar, around 2.0, 2.2, and 0.0 Å, respectively. The two exceptions are Ca and Cd ions, whose M—N(Pph) and M—Plane distances are much longer than those of the other complexes. For example, in the p0 case, Ca does not like to stay inside the inner cavity of the porphyrin ring, and instead it opts to lie 0.874 Å outside the porphyrin plane. In the p1 case, after one pyridine group binds axially to the metal ion, the Ca ion moves further away

TABLE 1: Selected Structural Parameters from the Optimized Structure of the Three Categories of Heme Complexes with 11 Divalent Metal Ions^a

Py no.	distance (Å)	Mg	Ca	Cr	Mn	Fe	Co	Ni	Cu	Zn	Ru	Cd
0	multiplicity	1	1	5	6	3	2	1	2	1	3	1
	M–N(Pph)	2.069	2.298	2.053	2.094	2.010	1.993	1.982	2.029	2.059	2.060	2.155
	M–Plane	0.005	0.874	0.004	0.015	0.007	0.006	0.014	0.003	0.005	0.008	0.121
1	multiplicity	1	1	5	6	3	2	3	2	1	1	1
	M–N(Pph)	2.100	2.320	2.064	2.135	2.023	2.010	2.065	2.041	2.092	2.064	2.213
	M–N(Py)	2.245	2.559	2.526	2.291	2.346	2.253	2.115	2.569	2.249	2.006	2.420
2	M–Plane	0.335	0.936	0.120	0.410	0.120	0.112	0.234	0.114	0.314	0.140	0.562
	multiplicity	1		3	6	1	2	3	2	1	1	
	M–N(Pph)	2.093		2.147	2.116	2.030	2.014	2.070	2.043	2.084	2.068	
	M–N(Py)	2.410		2.052	2.521	2.068	2.393	2.276	2.751	2.493	2.124	
	M–Plane	0.002		0.008	0.034	0.110	0.007	0.009	0.011	0.014	0.003	
divalent ionic radius (Å)		0.65	0.99	0.84	0.80	0.76	0.74	0.72	0.72	0.74	0.77	0.97

^a “M–N(Pph)” stands for the average bond length of metal ion–porphyrin nitrogen bond distance; “M–N(Py)” denotes the average bond length of the metal ion–pyridine nitrogen bond; and “M–Plane” represents the out-of-plane distance of the metal ion from the porphyrin plane.

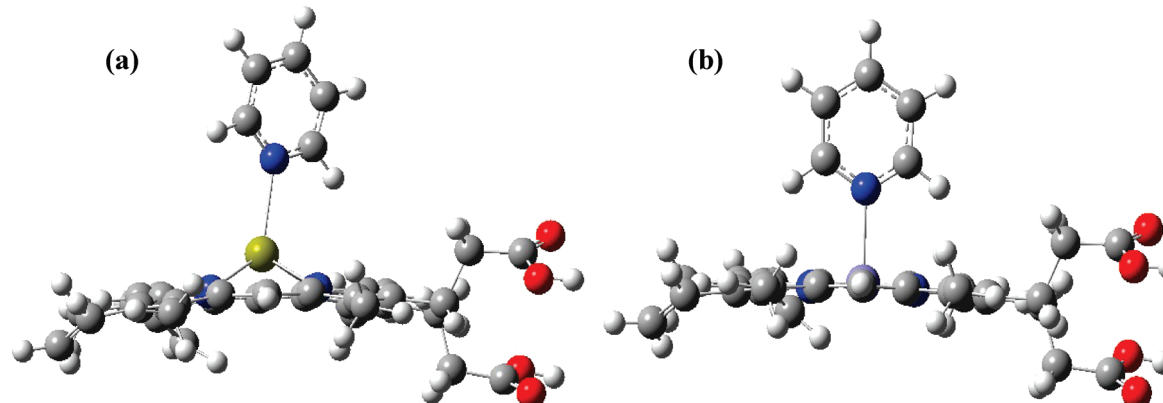


Figure 1. Comparison of the optimized structures for the p1 system between (a) pyridine–Ca(II)–porphyrin and (b) pyridine–Fe(II)–porphyrin complexes, where the main differences are that (i) Ca(II) stays outside of the porphyrin plane with Fe(II) residing in the inner cavity of the porphyrin plane and (ii) the pyridine ring of the Ca(II) complex is leaning toward the carboxyl groups.

from the porphyrin ring, preventing the second pyridine group from axially binding to the metal ion on the other side of the ring. Figure 1 shows the optimized structures for the p1 system of Ca–porphyrin and Fe–porphyrin complexes: one can see that the main differences between the two structures lies in that (i) the Ca cation in Figure 1a stays outside of the porphyrin plane whereas in Figure 1b the iron ion resides inside the inner cavity of the porphyrin plane and (ii) the pyridine ring of the Ca structure in Figure 1a is leaning toward the carboxyl groups whereas in Figure 1b the pyridine ring holds at the upright position perpendicular to the porphyrin plane. The same is true for the Cd case. The large M–Plane distance of Ca and Cd complexes explains why no stable p2 complex has been obtained in our calculations for these two metal ions.

Why do divalent Ca and Cd ions tend to move out of the porphyrin plane, but other metal ions do not? One can find the answer from the ionic radii tabulated in Table 1. These metal ions are considerably larger in size than others, so much so that the inner cavity of the porphyrin ring does not have enough space to accommodate them. Since two axial ligands are required for the porphyrin–metal complex in proteins to function properly under physiological conditions, these results justify the experimental finding that no porphyrin complex with Ca or Cd has been detected in nature. These results also suggest that the exclusion, rather than selection, of larger metal ions such as Ca and Cd from porphyrin metalation is a consequence of the fact that they simply cannot form stable structures with two axial ligands.

Another structural feature of the (pyridine)_n–metal–porphyrin system is the orientation of the pyridine ring relative to the

porphyrin plane. In both p1 and p2 cases, the axially bonded pyridine ring is perpendicular to the porphyrin plane. In principle, these pyridine rings can freely rotate along the metal–pyridine bond. In Figure 2, using Fe(II) as an example, we plotted the flexible scan PES (potential energy surface) results of the above rotation for both p1 (Figure 2a) and p2 (Figure 2b) systems. It was observed that marginal energy differences of up to a few kilocalories/mole can be obtained as the pyridine ring perpendicularly rotates above or underneath the Fe–porphyrin plane. Notice that in order to obtain Figure 2b, in other words, for the second pyridine ring to rotate, we have fixed the first pyridine ring at its optimal position obtained from Figure 2a. We chose the most stable conformer in our later studies.

The most common porphyrin binding metal in nature is the iron ion. Does Table 1 provide any structural information about why iron is favored? From the bond length data, no apparent pattern can be identified. However, we find that the one major difference between Fe and other metals in the table is the multiplicity change from open-shell in p1 to close-shell in p2. No other metal ion in Table 1 experiences such an open-to-close-shell transition from p1 to p2, although we noticed the same change for Ru from p0 to p1. Whether or not this spin-state related effect⁴⁴ is unique to iron and whether or not this change is essential for porphyrin complexes to properly function in physiological conditions remains to be investigated in future studies. But as will be shown below from NBO analyses and conceptual DFT descriptor results, the iron–porphyrin complex does demonstrate some unique behaviors in comparison with

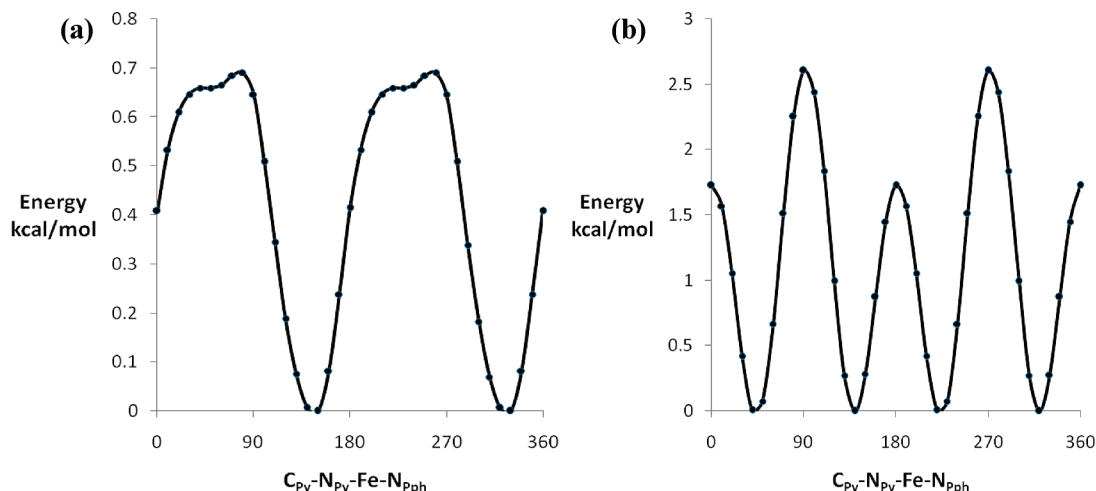


Figure 2. Potential energy surface scanned by the vertical rotation of the pyridine ring over the plane of the Fe–porphyrin complex for p1 (a) and p2 (b) classes. The x-axis is the $C_{Py}-N_{Py}-Fe-N_{Pph}$ angle, and the y-axis is the energy difference in kcal/mol. In the p2 case, we fixed the first pyridine in the lowest-energy conformation and allowed the second pyridine ring to axially rotate on the other side of the Fe–porphyrin plane.

TABLE 2: NBO Charge Distribution and Second-Order Perturbation Theory Analyses of the Three Systems in Scheme 1.^a

py no.	type	Mg	Ca	Cr	Mn	Fe	Co	Ni	Cu	Zn	Ru	Cd
0	M	1.753	1.788	1.268	1.518	1.075	1.079	1.018	1.304	1.620	0.898	1.609
	N (Pph)	-0.726	-0.696	-0.626	-0.680	-0.588	-0.588	-0.558	-0.626	-0.702	-0.539	-0.687
	Pph→M	153.3	99.2	517.0	320.8	434.7	404.5	392.2	289.8	230.9	709.2	397.1
	M→Pph	5.2	35.0	147.7	153.4	268.6	131.3	229.4	71.4	13.8	2056.7	312.6
1	M	1.742	1.765	1.245	1.463	1.126	1.082	1.439	1.333	1.695	0.713	1.642
	N(Py)	-0.560	-0.556	-0.490	-0.537	-0.488	-0.478	-0.501	-0.486	-0.545	-0.323	-0.547
	N(Pph)	-0.700	-0.673	-0.612	-0.655	-0.571	-0.557	-0.623	-0.618	-0.682	-0.490	-0.672
	Pph→M	185.1	121.0	596.8	384.2	533.7	214.8	359.3	293.2	253.2	956.6	395.7
2	M→Pph	228.2	143.9	401.2	475.0	456.4	260.0	339.3	224.4	59.5	5284.9	770.5
	Py→M	29.7	17.0	7.2	57.0	12.1	14.6	18.4	17.9	32.7	15.5	45.3
	M→Py	34.9	43.8	42.9	91.7	30.1	25.3	25.2	18.0	10.9	609.2	125.5
	M	1.736		1.273	1.391	0.747	1.043	1.320	1.352	1.644	0.549	
	N(Py)	-0.512		-0.456	-0.488	-0.400	-0.459	-0.475	-0.462	-0.495	-0.374	
	N(Pph)	-0.689		-0.600	-0.643	-0.506	-0.544	-0.610	-0.616	-0.681	-0.467	
	Pph→M	119.2		1035.2	480.9	901.8	538.6	389.1	274.3	262.4	1467.7	
	M→Pph	266.6		1369.8	505.0	1340.0	600.4	554.5	317.1	184.0	7251.2	
	Py→M	47.8		156.8	18.6	265.2	27.6	81.2	13.9	47.5	397.4	
	M→Py	70.6		301.5	90.7	502.3	88.7	162.1	35.5	29.1	811.7	

^a Charges listed are those on the metal ion, M, and nitrogen atoms of porphyrin, N(Pph), and pyridine, N(Py). L→M stands for the donor–acceptor interaction between L (porphyrin and pyridine) and M (metal), where L serves as the electron donor and M as the electron acceptor. The total interaction, in kcal/mol, is the sum of all orbital contributions larger than 0.05 kcal/mol.

other metal complexes in terms of its electronic structure and reactivity properties.

Table 2 exhibits the charge distribution for a selected list of atoms obtained from the NBO analyses.³⁷ Also shown in the table are the donor–acceptor back-bonding interactions for pairs such as porphyrin (donor)→metal (acceptor), metal (donor)→porphyrin (acceptor), etc. These pairs, obtained from the second-order perturbation theory analysis of the Fock matrix in the NBO basis, provide the hyperconjugation or back-bonding interaction energies between different chemical motifs in a complex. From the table, one finds that positive charges on Mg, Ca, Zn, and Cd are relatively larger than others, and their corresponding N(Pph) atoms are more negatively charged, indicating that their M–N(Pph) bonds are more ionic. On the other hand, Fe, Co, Ni, and Ru ions, especially Ru, and their corresponding N(Ppy) atoms have relatively smaller NBO charges, meaning that these M–N(Ppy) bonds possess a relatively larger component of covalent bonding. Taking a look at the charge change from p1 to p2 on the metal ion, we noticed that for most of the complexes not much variation takes place during the transition, with the charge changes on metals all being less than 0.1. The two exceptions are Fe and Ru where the charge decreased by about

0.4 and 0.2, respectively, from p1 to p2. Since p2 is the active state for porphyrin complexes to undertake catalytic functions in proteins, this large reduction of charge on the heme reaction center may well be a prerequisite of the catalyst, thus providing clues to why the Fe ion is favored over others for porphyrin metalation in hemoproteins.

Also shown in Table 2 are the donor–acceptor back-bonding interactions between porphyrin and the metal ion (Pph→M, where porphyrin is a donor and the metal is an acceptor, and M→Pph, where the metal acts as a donor and porphyrin as an acceptor) and between pyridine and the metal ion (Py→M, where pyridine is the donor and the metal is the acceptor, and M→Py, where the metal acts as a donor and pyridine as its acceptor). The general trend is that these interaction energies are larger for transition metals (e.g., Fe, Co, and Ni) and smaller for those without d electrons (e.g., Mg and Ca) or whose d orbitals are full (e.g., Zn). Large back-bonding energies from the fifth-period Ru complex account for the fact that it has a smaller charge distribution and larger covalent contributions. Looking at the M→Py and Py→M energies of the first-row transition metal ions for p2, we find that Fe has the largest sum of these back-bonding interactions. This strong interaction

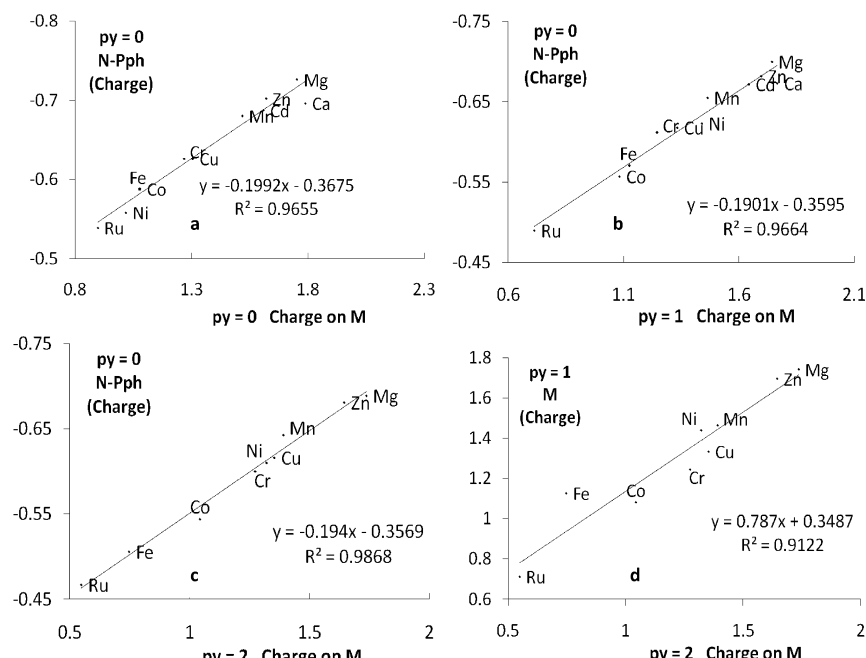


Figure 3. Strong linear relationships between charge distributions of metal ion and porphyrin's nitrogen atoms in different complex systems.

TABLE 3: Global Reactivity Descriptors From Conceptual DFT Including Frontier Orbitals HOMO and LUMO, Chemical Potential μ , Global Hardness η , and Electrophilicity Index ω for the Three Categories of Systems (Units in au)

py no.	indicators	Mg	Ca	Cr	Mn	Fe	Co	Ni	Cu	Zn	Ru	Cd	average
0	HOMO	-0.188	-0.182	-0.188	-0.157	-0.188	-0.188	-0.189	-0.189	-0.189	-0.178	-0.191	-0.184
	LUMO	-0.082	-0.077	-0.086	-0.087	-0.087	-0.090	-0.079	-0.083	-0.081	-0.104	-0.084	-0.085
	μ	-0.135	-0.130	-0.137	-0.122	-0.138	-0.139	-0.134	-0.136	-0.135	-0.141	-0.138	-0.135
	η	0.106	0.105	0.102	0.070	0.101	0.099	0.110	0.106	0.108	0.073	0.107	0.099
	ω	0.086	0.080	0.092	0.105	0.094	0.098	0.082	0.088	0.084	0.136	0.088	0.094
1	HOMO	-0.178	-0.173	-0.160	-0.15	-0.164	-0.180	-0.179	-0.183	-0.177	-0.174	-0.176	-0.172
	LUMO	-0.073	-0.069	-0.079	-0.075	-0.079	-0.072	-0.072	-0.075	-0.071	-0.070	-0.073	-0.073
	μ	-0.126	-0.121	-0.120	-0.113	-0.122	-0.126	-0.126	-0.129	-0.124	-0.122	-0.125	-0.123
	η	0.105	0.104	0.081	0.075	0.085	0.108	0.107	0.108	0.106	0.104	0.103	0.099
	ω	0.075	0.070	0.088	0.084	0.087	0.074	0.074	0.077	0.073	0.072	0.075	0.077
2	HOMO	-0.172		-0.115	-0.129	-0.173	-0.175	-0.171	-0.178	-0.173	-0.165		-0.161
	LUMO	-0.070		-0.075	-0.073	-0.066	-0.067	-0.069	-0.070	-0.069	-0.064		-0.069
	μ	-0.121		-0.095	-0.101	-0.120	-0.121	-0.120	-0.124	-0.121	-0.115		-0.115
	η	0.102		0.040	0.056	0.107	0.108	0.102	0.108	0.104	0.101		0.092
	ω	0.072		0.113	0.091	0.067	0.068	0.070	0.071	0.070	0.065		0.076

between the Fe ion and axial ligands elucidates why there is a substantial decrease of the NBO charge on Fe from p1 to p2. This substantial enhancement of interactions in p2 may also be an indication of the uniqueness of this metal ion in forming complexes with porphyrin.

In Figure 3, we plotted four linear relationships between the charge distributions of metal ions M and porphyrin's nitrogen atoms. Ionic bonds have larger positive charges on M and more negative charges on N–Pph, which are represented by the Mg, Ca, and Zn data points at the top right of the lines. On the other hand, more covalently bonded systems have the metal ion and nitrogen atom less charged, represented by the Ru and Fe data points sitting at the lower left-hand corner of the lines. From the lines in Figure 3, we find that the charge distributions among different systems correlate well with each other. One outlier in Figure 3d is Fe, for which, as mentioned earlier, due to the enhanced back-bonding interaction between Fe and the axial pyridine groups, a drastic change in NBO charge is observed.

Global descriptors from conceptual DFT including HOMO/LUMO, chemical potential, hardness, and electrophilicity index for the three classes of metal–porphyrin complexes are tabulated in Table 3. We found that the HOMO and LUMO energies do

not change markedly with different metal complexes within each of the classes of compounds, except Mn, whose HOMO energy is much higher than that of the others (most likely due to its higher multiplicity). Since the HOMO and LUMO energies are similar among different metal complexes in each category, so are the other conceptual DFT descriptors derived from them. However, from p0 to p1 and p1 to p2, as can be seen from the average value (the last column of Table 3), one finds that both HOMO and LUMO energies become monotonically higher. This leads to the conclusion that, in general, chemical potential becomes higher, hardness smaller, and electrophilicity index smaller. Since hardness is an indication of molecular stability, the smaller the hardness the less stable the system becomes; the general picture of p0 to p1 to p2 transitions demonstrates that the system becomes more reactive as more axial ligands bind to the metal ion inside the porphyrin ring. On the other hand, the smaller average electrophilicity value in Table 3 suggests that the system, in the meantime, also becomes less reactive toward accepting electrons. The results from hardness and electrophilicity seem to contradict each other: the system becomes less stable from p0 to p2 but less reactive in accepting electrons at the same time. As will be discussed below with

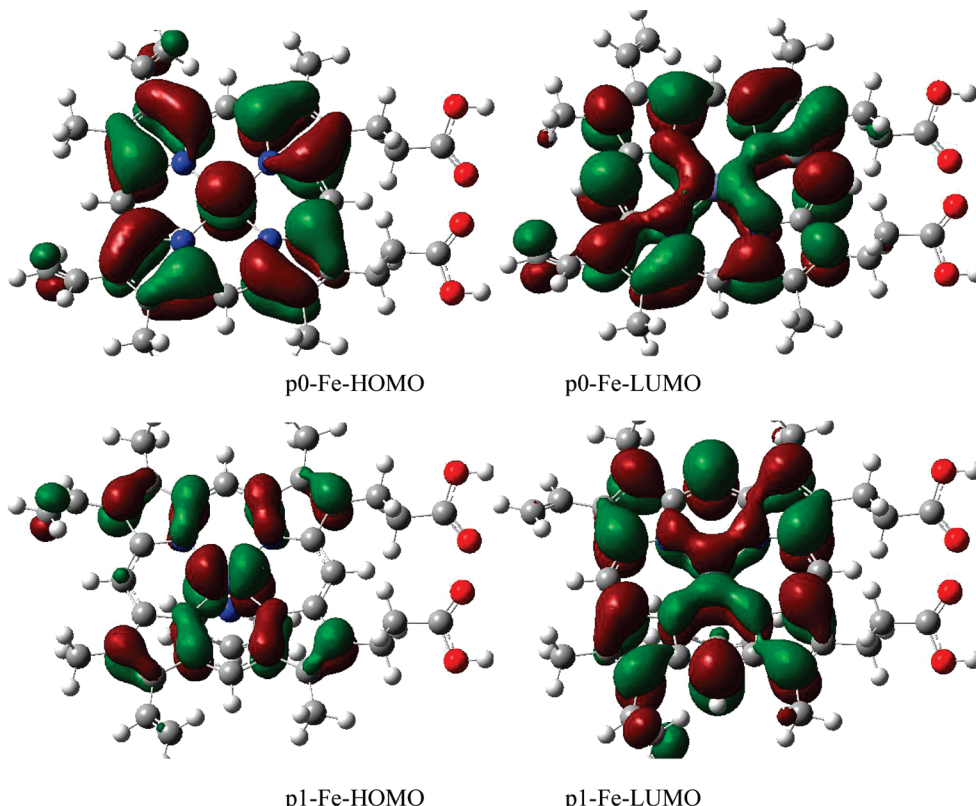


Figure 4. HOMO and LUMO contour surfaces of p0 and p1 Fe-porphyrin systems.

TABLE 4: Local Reactivity Descriptors, Fukui Function and Dual Descriptor, From Conceptual DFT for a Few Selected Atomic Sites of the Three Classes of Porphyrin-Metal Complexes Studied^a

py no.	indicators	Mg	Ca	Cr	Mn	Fe	Co	Ni	Cu	Zn	Ru	Cd
1	f_M^+	0.005	0.013	0.036	0.269	0.067	0.398	0.008	0.373	0.008	0.226	0.009
	f_M^-	0.004	0.007	0.207	0.122	0.015	0.267	0.009	0.005	0.002	0.321	0.005
	$f_M^{(2)}$	0.001	0.006	-0.171	0.147	0.052	0.131	-0.001	0.368	0.006	-0.095	0.004
	$f_{N-Pph}^{(2)}$	0.029	0.027	0.007	-0.105	0.014	-0.055	0.027	-0.037	0.028	-0.022	0.028
	f_M^+	0.003	0.007	0.030	0.308	0.065	0.006	-0.002	0.357	0.004	0.002	0.005
	f_M^-	0.000	0.004	0.268	0.116	0.294	0.152	0.007	0.005	0.003	0.258	0.001
2	$f_M^{(2)}$	0.003	0.003	-0.238	0.192	-0.229	-0.146	-0.009	0.352	0.001	-0.256	0.004
	$f_{N-Pph}^{(2)}$	0.027	0.022	0.022	-0.097	0.018	0.024	-0.025	-0.070	0.029	0.032	0.027
	$f_{N-py}^{(2)}$	0.006	0.043	-0.037	0.002	0.000	0.004	0.000	-0.029	0.004	0.026	0.005
	f_M^+	0.002		0.064	0.079	-0.003	0.004	-0.001	0.333	0.003	0.004	
	f_M^-	0.004		0.086	0.123	0.286	0.127	-0.008	0.008	-0.001	0.442	
	$f_M^{(2)}$	-0.002		-0.022	-0.044	-0.289	-0.123	0.007	0.325	0.004	-0.438	
3	$f_{N-Pph}^{(2)}$	-0.035		0.003	-0.086	0.046	0.024	-0.036	-0.011	0.028	0.063	
	$f_{N-py}^{(2)}$	0.003		0.005	0.015	0.006	-0.067	0.000	-0.022	0.001	0.021	

^a The symbols f_M^+ and $f_M^{(2)}$ denote Fukui function and dual descriptor of the metal ion, respectively; f_{N-Pph} and $f_{N-Pph}^{(2)}$ represent the average Fukui function of four nitrogens in the porphyrin; and f_{N-py} and $f_{N-py}^{(2)}$ stand for average Fukui function of the nitrogen atoms in two pyridines in p2 or the one in p1. Units in au.

the dual descriptors, the reactivity that matters most to the metal-porphyrin complex in carrying out proper catalytic functions in proteins is not electrophilicity but nucleophilicity (the capability of donating electrons) since in the early steps of its catalytic loop divalent Fe(II) will be oxidized to Fe(IV).

For Fe complexes, from p0 to p1, conceptual DFT descriptors follow the average pattern of HOMO/LUMO; μ values increased; and η and ω values decreased. Figure 4 shows the HOMO and LUMO contour surfaces for p0 and p1, from which it is seen that the shapes of the LUMO do not change considerably during the transition, whereas substantial differences between p0 and p1 are seen for the HOMO. This is consistent with the results of the second-order perturbation theory and the nucleophilic nature of its reactivity. Deviations from the average picture in Table 3 are seen for the p2 Fe

complex where a much smaller ω and relatively larger η is observed, which suggests that, compared to other metal complexes, the Fe complex is more stable and less reactive in electron-accepting reactions. The greater stability as well as the larger nucleophilic reactivity (as will be shown below) relative to other metal complexes is another prominent feature of the iron-porphyrin complex.

Table 4 shows local reactivity descriptors from conceptual DFT for a few key atomic sites of the systems. Recall that the dual descriptor $f^{(2)}(r)$ is defined as the difference between the nucleophilic Fukui function, $f^+(r)$, and the electrophilic Fukui function, $f^-(r)$, under the finite difference approximation and that it is positive in electrophilic (electron-accepting) regions and negative in nucleophilic (electron-donating) regions. In the p0 case, as shown in the table, $f_M^{(2)}$ is positive and thus

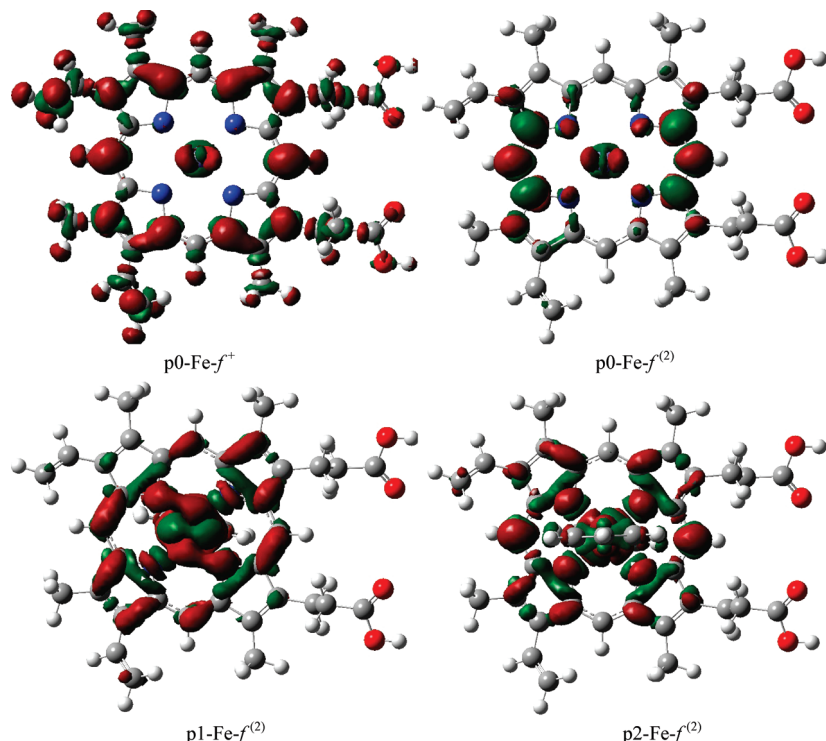


Figure 5. Fukui function and dual descriptor of p0, p1, and p2 Fe–porphyrin systems.

electrophilic except for Cr, Ni, and Ru complexes. This electrophilic nature of $f_M^{(2)}$ switches to having an electron-donating, nucleophilic nature in p1 and p2 cases for most systems, which is essential for the complex to perform biological functions after axial ligands are bonded to the metal–porphyrin complex. Notice in particular that in the p2 case Fe and Ru complexes possess the largest magnitude of the nucleophilic dual descriptor $f_M^{(2)}$, indicating that these two metal complexes have the largest capacity for providing electrons to other species involved in the catalytic reaction. To differentiate Fe from other metal ions from the point of view of reactivity, these data offer another piece of strong evidence to substantiate the fact that

porphyrin naturally prefers to metalate with the iron ion in hemoproteins. We also noticed that the magnitudes of $f_{N-PPh}^{(2)}$ and $f_{N-py}^{(2)}$ are relatively small, and thus these sites are expected to be uneventful during the catalytic process.

Figure 5 displays the dual descriptors of p0, p1, and p2 for the Fe complex. For comparison purposes we also plotted one Fukui function of p0. It can be seen that the dual descriptors are much more localized than the corresponding Fukui function. Moreover, we observe that from p0 to p1 more distributions of the dual descriptor are concentrated on the metal ion region, confirming what we discovered and discussed from the data in

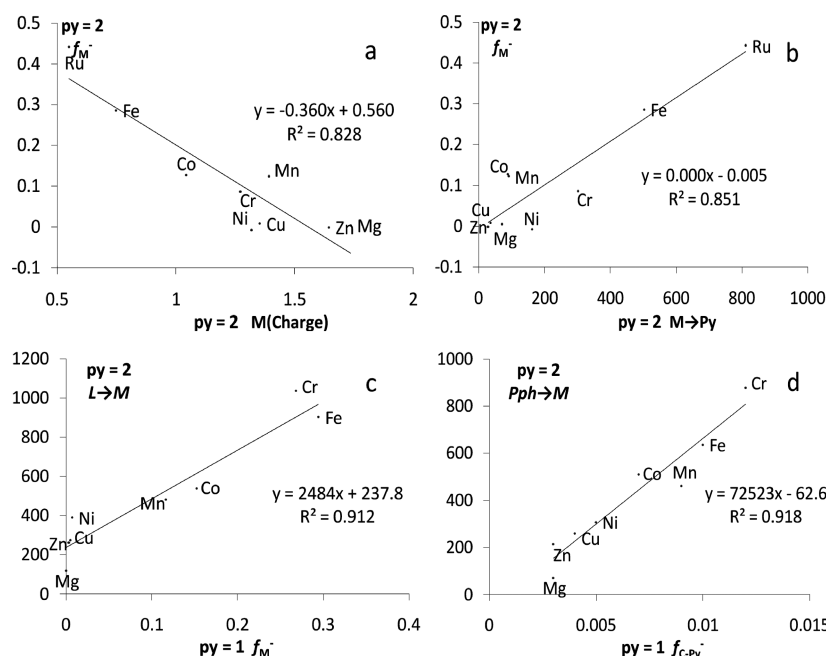


Figure 6. Linear relationships between structure and conceptual DFT reactivity properties for p1 and p2 metal–porphyrin complexes.

Table 4 that the transition leads to a switch of the metal ion's reactivity nature from electrophilic to nucleophilic.

Figure 6 exhibits a few linear correlations between the structural and reactivity properties obtained from this study, including Fukui function, f_M^- , vs NBO charge on the metal ion (Figure 6a), M→Py backbonding interactions (Figure 6b) of p2, f_M^- of p1 vs L (sum of Py and Pph)→M backbonding energy of p2 (Figure 6c), and f_{C-Py}^- of p1 vs Pph→M energy (Figure 6d). These reasonable correlations suggest that the structural and reactivity properties of the metal-porphyrin complexes are interrelated. These relationships also confirm the findings from the present study that we discussed above. For example, in Figure 6a, we find that both Fe and Ru are least charged positively in p2, and thus they are most nucleophilic, as shown by the f_M^- Fukui function, which is a measure of the regioselective susceptibility to electron donation. In Figure 6b, the linear relationship between M→Py energy and f_M^- demonstrates that the strong nucleophilicity of Fe and Ru comes from the strong backbonding interaction from the metal ion to the axial pyridine ring. Figures 6c and 6d illustrate some cross-system correlations between Fukui functions of the p1 system and backbonding interactions in the p2 system. Figure 6c showcases the strong correlation between the Fukui function on the metal cation f_M^- in p1 and the total backbonding interaction from ligand (porphyrin and pyridine) to the metal cation on p2. They are directly related; that is, the larger the f_M^- in p1 the larger the energy of L→M in p2. This is understandable since a larger f_M^- in p1 indicates that it has a better capability to accept more electrons when more electrons are made available from extra ligands. Figure 6d reveals the strong correlation between the Fukui function f_{C-Py}^- (average Fukui function of pyridine's carbon atoms) in p1 and the back-bonding interaction from the porphyrin ring to the metal ion of p2. This correlation is not at all obvious nor trivial. These results provide illustrative examples, suggesting that structural and reactivity properties of simpler systems can be descriptors or indicators of structural and reactivity properties of more complicated ones.

4. Summary and Concluding Remarks

Porphyrin complexed with one divalent metal cation is one of the key cofactors in hemoproteins. While the iron ion is the most abundant and common species to metalate with porphyrin, other metal forms in the complex have also been detected. How the metal ion affects the porphyrin complex's structure and reactivity and why certain metals can complex with porphyrin but others cannot are still up to debate. These and other relevant questions can be addressed using theoretical and computational methods to understand metal selectivity and the specificity of porphyrin. Toward that end, the structural and reactivity properties of a series of (pyridine)_n-M(II)-porphyrin complexes with M = Mg, Ca, Cr, Mn, Fe, Co, Ni, Cu, Zn, Ru, and Cd and n = 0, 1, and 2 have systematically been investigated by DFT and conceptual DFT approaches in the present work.

We found that the exclusion of larger metal ions, such as Ca and Cd, complexed with porphyrin can be attributed to structural difficulties, namely, that these metal ions cannot form stable structures when two axial ligands are bonded to the metal center of the metal-porphyrin complex due to the fact that these ions are larger in size and cannot reside in the inner cavity of the porphyrin ring. As to why iron is preferred over other transition metals, data from the second-order perturbation theory analysis of the Fock matrix in the NBO basis and conceptual DFT reactivity descriptors such as hardness, electrophilicity, and dual descriptors have provided pieces of strong evidence and

meaningful insights. It has been revealed that the iron complex differs from other metal ion complexes in bonding and reactivity properties (i.e., charge distribution, stability, and nucleophilicity) when two axial bonds are formed, enhancing and facilitating the role of the iron cation as the center of the catalytic process. These results imply that the number and nature of the axial ligands also play an important role in the catalytic process.

Finally, we noticed in passing that the behaviors of Ru and Fe (both from the same periodic group) complexes are similar from the perspective of their structural and reactivity properties. While other factors such as reaction thermodynamics and kinetics may come into play to separate the two, the scarcity of Ru in nature can alone validate why nature favors iron over Ru in hemoproteins. On the other hand, this similarity might provide us with meaningful options in the chemical modification of hemoproteins. In addition, we note that spin polarization also plays an important role in metal specificity and reactivity. These and other relevant issues will be addressed in our future work.

Acknowledgment. This work was financially supported in part by the National Natural Science Foundation of China (grant Nos. 20573011, 20733002, and 20873008) and Major State Basic Research Development Programs (grant Nos. 2004CB719903 and 2002CB613406). Helpful discussion with Robert G. Parr of University of North Carolina at Chapel Hill is gratefully acknowledged.

References and Notes

- (1) Perutz, M. F. *Nature* **1970**, 228, 726.
- (2) Monod, J.; Wyman, J.; Changeux, J. P. *J. Mol. Biol.* **1965**, 12, 88.
- (3) Wittenberg, B. A.; Wittenberg, J. B. *Annu. Rev. Physiol.* **1989**, 51, 857.
- (4) Qiu, Y.; Sutton, L.; Riggs, A. F. *J. Biol. Chem.* **1998**, 273, 23426.
- (5) Wilcox, D. E.; Porras, A. G.; Hwang, Y. T.; Lerch, K.; Winkler, M. E.; Solomon, E. I. *J. Am. Chem. Soc.* **1985**, 107, 4015.
- (6) Winkler, M. E.; Lerch, K.; Solomon, E. I. *J. Am. Chem. Soc.* **1981**, 103, 7003.
- (7) Himmelwright, R. S.; Eickman, N. C.; LuBien, C. D.; Solomon, E. I.; Lerch, K. *J. Am. Chem. Soc.* **1980**, 102 (24), 7339.
- (8) Burmester, T.; Weich, B.; Reinhardt, S.; Hankeln, T. *Nature* **2000**, 407, 520.
- (9) Hardison, R. C. *Proc. Natl. Acad. Sci. U.S.A.* **1996**, 93, 5675.
- (10) Spiro, T. G.; Jarzecki, A. A. *Curr. Opin. Chem. Biol.* **2001**, 5, 715.
- (11) Ortiz de Montellano, P. R. *Cytochrome P450: Structure, Mechanism and Biochemistry*, 3rd ed.; Kluwer Academic/Plenum: New York, 2005.
- (12) Sigel, A.; Sigel, H.; Sigel, R. K. O. Eds. *Ubiquitous Roles of Cytochrome P450 Proteins. Metal Ions in Life Science*; John Wiley & Sons Ltd.: West Sussex, U.K., 2007; Vol. 3.
- (13) Sono, M.; Roach, M. P.; Coulter, E. D.; Dawson, J. H. *Chem. Rev.* **1996**, 96, 2841.
- (14) Meunier, B. *Chem. Rev.* **1992**, 92, 1411.
- (15) Jordan, P.; Fromme, P.; Witt, H. T.; Klukas, O.; Seanger, W.; Krauß, N. *Nature* **2001**, 411, 909.
- (16) Kang, S. A.; Marjavaara, P. J.; Crane, B. R. *J. Am. Chem. Soc.* **2004**, 126 (35), 10836.
- (17) Tsutsui, M.; Ichikawa, M.; Vohwinkel, F.; Suzuki, K. *J. Am. Chem. Soc.* **1966**, 88, 854.
- (18) Donato, R. *Biochim. Biophys. Acta* **1999**, 1450, 191.
- (19) Schafer, B. W.; Heizmann, C. W. *Trends Biochem. Sci.* **1996**, 21, 134.
- (20) Zimmer, D. B.; Cornwall, E. H.; Landar, A.; Song, W. *Brain Res. Bull.* **1995**, 37, 417.
- (21) Auld, D. S. *BioMetals* **2001**, 14, 271.
- (22) Klug, A.; Rhodes, D. *Trends Biochem. Sci.* **1987**, 12, 464.
- (23) Payre, F.; Vincent, A. *FEBS Lett.* **1988**, 234, 245.
- (24) Klevit, R. E. *Science* **1991**, 253, 1367.
- (25) Klug, A. *J. Mol. Biol.* **1999**, 293, 215.
- (26) Parr, R. G.; Yang, W. *Density Functional Theory of Atoms and Molecules*; Oxford University Press: Oxford, U.K., 1989. Liu, S. B.; Parr, R. G. *J. Chem. Phys.* **1997**, 106, 5578.

- (27) Geerlings, P.; De Proft, F.; Langenaeker, W. *Chem. Rev.* **2003**, *103*, 1793. Chattaraj, P. K.; Sarkar, U.; Roy, D. R. *Chem. Rev.* **2006**, *106*, 2065. Liu, S. *Acta Phys. Chim. Sin.* **2009**, *25*, 590.
- (28) Huang, Y.; Zhong, A. G.; Rong, C. Y.; Xiao, X. M.; Liu, S. B. *J. Phys. Chem. A* **2008**, *112*, 305. Zhong, A. G.; Rong, C. Y.; Liu, S. B. *J. Phys. Chem. A* **2007**, *111*, 3132. Liu, S. B.; Govind, N. *J. Phys. Chem. A* **2008**, *112*, 6690. Liu, S. B.; Govind, N.; Pedersen, L. G. *J. Chem. Phys.* **2008**, *129*, 094104. Roy, D. R.; Chattaraj, P. K. *J. Phys. Chem. A* **2008**, *112*, 1612. Xia, Y.; Yin, D. L.; Rong, C. Y.; Xu, Q.; Yin, D. H.; Liu, S. B. *J. Phys. Chem. A* **2008**, *112*, 9970. Liu, S. B.; Pedersen, L. G. *J. Phys. Chem. A* **2009**, *113*, 3648. Torrent-Sucarrat, M.; Liu, S. B.; De Proft, F. *J. Phys. Chem. A* **2009**, *113*, 3698. Li, T.; Ayers, P. W.; Liu, S. B.; Swadley, M. J.; Aubrey-Medendorp, C. *Chem.—Eur. J.* **2009**, *15*, 361. Ugur, I.; Vleeschouwer, F. D.; Tuzun, N.; Aviyente, V.; Geerlings, P.; Liu, S. B.; Ayers, P. W.; De Proft, F. *J. Phys. Chem. A* **2009**, *113*, 8704.
- (29) Mulliken, R. S. *J. Chem. Phys.* **1934**, *2*, 782.
- (30) Janak, J. F. *Phys. Rev. B* **1978**, *18*, 7165.
- (31) Parr, R. G.; Szentpály, L. V.; Liu, S. B. *J. Am. Chem. Soc.* **1999**, *121*, 1922. Liu, S. B. Electrophilicity. In: *Chemical reactivity theory: a density functional theory view*; Chattaraj, P. K., Ed.; Taylor & Francis Group: London, 2009.
- (32) Ayers, P. W.; Anderson, J. S. M.; Rodriguez, J. I.; Jawed, Z. *Phys. Chem. Chem. Phys.* **2005**, *7*, 1918. Ayers, P. W.; Anderson, J. S. M.; Bartolotti, L. J. *Int. J. Quantum Chem.* **2005**, *101*, 520.
- (33) Parr, R. G.; Yang, W. *J. Am. Chem. Soc.* **1984**, *106*, 4049. Ayers, P. W.; Levy, M. *Theor. Chem. Acc.* **2000**, *103*, 353.
- (34) Yang, W.; Mortier, W. J. *J. Am. Chem. Soc.* **1986**, *108*, 5708.
- (35) Lee, C.; Yang, W.; Parr, R. G. *J. Mol. Struct. (THEOCHEM)* **1988**, *163*, 305.
- (36) Gaenko, A. V.; Devarajan, A.; Trifonov, E.; Ostrovskii, V. A. *J. Phys. Chem. A* **2006**, *110*, 8750. Roos, G.; Loverix, S.; De Proft, F.; Wyns, L.; Geerlings, P. *J. Phys. Chem. A* **2003**, *107*, 6828.
- (37) Morell, C.; Grand, A.; Toro-Labbe, A. *J. Phys. Chem. A* **2005**, *109*, 205. Ayers, P. W.; Morell, C.; De Proft, D.; Geerlings, P. *Chem.—Eur. J.* **2007**, *13*, 8240. Geerling, P.; De Proft, F. *Phys. Chem. Chem. Phys.* **2008**, *10*, 3028.
- (38) Reed, A. E.; Curtiss, L. A.; Weinhold, F. *Chem. Rev.* **1988**, *88*, 899.
- (39) Becke, A. D. *Phys. Rev. A* **1988**, *38*, 3098–3100. Becke, A. D. *J. Chem. Phys.* **1993**, *98*, 5648.
- (40) Lee, C.; Yang, W.; Parr, R. G. *Phys. Rev. B* **1988**, *37*, 785.
- (41) Krishnan, R.; Binkley, J. S.; Seeger, R.; Pople, J. A. *J. Chem. Phys.* **1980**, *72*, 650.
- (42) Frisch, M. J.; Pople, J. A.; Binkley, J. S. *J. Chem. Phys.* **1984**, *80*, 3265.
- (43) Zhang, R. Q.; Huang, J. H.; Bu, Y. X.; Han, K. L.; Lee, S. T.; He, G. Z. *Sci. China, Ser. B* **2000**, *43*, 375.
- (44) Fan, W. J.; Zhang, R. Q.; Liu, S. B. *J. Comput. Chem.* **2007**, *28*, 967. Rong, C.; Lian, S. X.; Yin, D. L.; Zhong, A. G.; Zhang, R. Q.; Liu, S. B. *Chem. Phys. Lett.* **2007**, *434*, 149.
- (45) Liu, S. B.; Langenaeker, W. *Theor. Chem. Acc.* **2003**, *110*, 338. Zhong, A. G.; Liu, S. B. *J. Theor. Comp. Chem.* **2005**, *4*, 833. Rong, C.; Lian, S.; Yin, D.; Shen, B.; Zhong, A. G.; Bartolotti, L.; Liu, S. B. *J. Chem. Phys.* **2006**, *125*, 174102.
- (46) Frisch, M. J.; Trucks, G. W.; Schlegel, H. B.; Scuseria, G. E.; Robb, M. A.; Cheeseman, J. R.; Montgomery, J. A., Jr.; Vreven, T.; Kudin, K. N.; Burant, J. C.; Millam, J. M.; Iyengar, S. S.; Tomasi, J.; Barone, V.; Mennucci, B.; Cossi, M.; Scalmani, G.; Rega, N.; Petersson, G. A.; Nakatsuji, H.; Hada, M.; Ehara, M.; Toyota, K.; Fukuda, R.; Hasegawa, J.; Ishida, M.; Nakajima, T.; Honda, Y.; Kitao, O.; Nakai, H.; Klene, M.; Li, X.; Knox, J. E.; Hratchian, H. P.; Cross, J. B.; Adamo, C.; Jaramillo, J.; Gomperts, R.; Stratmann, R. E.; Yazyev, O.; Austin, A. J.; Cammi, R.; Pomelli, C.; Ochterski, J. W.; Ayala, P. Y.; Morokuma, K.; Voth, G. A.; Salvador, P.; Dannenberg, J. J.; Zakrzewski, V. G.; Dapprich, S.; Daniels, A. D.; Strain, M. C.; Farkas, O.; Malick, D. K.; Rabuck, A. D.; Raghavachari, K.; Foresman, J. B.; Ortiz, J. V.; Cui, Q.; Baboul, A. G.; Clifford, S.; Cioslowski, J.; Stefanov, B. B.; Liu, G.; Liashenko, A.; Piskorz, P.; Komaromi, I.; Martin, R. L.; Fox, D. J.; Keith, T.; Al-Laham, M. A.; Peng, C. Y.; Nanayakkara, A.; Challacombe, M.; Gill, P. M. W.; Johnson, B.; Chen, W.; Wong, M. W.; Gonzalez, C.; Pople, J. A. *Gaussian 03*, revision E.01; Gaussian, Inc.: Pittsburgh, PA, 2003.

JP905885Y